Supplementary Information

Pt single atom alloyed sub-1 nm thick Fe overlayer on supported Cu nanoparticles for methylcyclohexane dehydrogenation

Akira Oda,[a]* Kosei Ichihashi,[a] Yuta Yamamoto,[b] Takeshi Ohtsu,[a] Wei Shi,[a] Kyoichi Sawabe,[a] Atsushi Satsuma[a]

[a]Department of Materials Chemistry, Graduate School of Engineering, Nagoya University, Furo-cho, Chikusa-ku, Nagoya 464-8603, Japan.

[b]Institute of Materials and Systems for Sustainability, Nagoya University, Nagoya 464-8603, Japan.

*Corresponding author: akira@chembio.nagoya-u.ac.jp

1. Methods

1.1. Materials.

$Pt(NO_3)_2$ (CATALER Co., Ltd, 8.6 wt% in HNO_3 solution), $Cu(NO_3)_2 \cdot 3H_2O$ (Kishida Chemical, >99.5%), $Fe(NO_3)_3 \cdot 9H_2O$ (Kishida Chemical, >99.0%), $Ni(NO_3)_2 \cdot 6H_2O$ (Kishida Chemical, >98.0%), $Co(NO_3)_2 \cdot 6H_2O$ (Kishida Chemical, >98.0%), $Zn(NO_3)_2 \cdot 6H_2O$ (Kishida Chemical, >99.0%), $In(NO_3)_3 \cdot 3H_2O$ (Kishida Chemical, >99.0%), $SnCl_2 \cdot 5H_2O$ (Kishida Chemical, >99.0%), $AgNO_3$ (Kishida Chemical, >99.8%), rutile TiO_2 (JRC-TIO-16), HNO_3 (Kishida Chemical, 60%), MCH (Kishida Chemical, >98.5%), TOL (Kishida Chemical, 99.5%), Ar (SogoKariya Sanso, 99.99%), H_2 (SogoKariya Sanso, 99.99%), CO (SogoKariya Sanso, >99.5%), O_2 (SogoKariya Sanso, 99.99%), O_2/He (SogoKariya Sanso, 20.0%), He (SogoKariya Sanso, 99.99%).

1.2. Catalyst preparation.

1.2.1. Supported Pt–FeCu SAA catalysts. The detailed experimental method was described in our previous work.[1] In short, a predetermined amount of 10 g/L $M(NO_3)_x$ aqueous solutions (M = Cu, Fe), r-TiO_2 (BET surface area: 36 m^2/g), and 50 mL distilled water were added to a flask that can be attached to an evaporator and stirred at room temperature for 1 h. The flask was attached to an evaporator and rotated in a water bath at 80°C, and the solution was removed by evacuation. The catalyst was further dried overnight at 80°C in air and subsequently calcined at 500°C at an increase rate of 10 °C/min for 1 h under the air. 200 mg of the dried catalyst was added to a 50 mL flask, and the temperature was raised to 500 °C at an increase rate of 10 °C/min under the 100 % H_2 flow at a rate of 20 mL/min and held for 1 h. After the reduction, the temperature was cooled to room temperature. The flask was then placed in ice water and cooled to 0 °C. Under the H_2 gas atmosphere, about 10 mL of distilled water was added to the flask to homogeneously disperse the catalyst. Then, 20 μl of 10 g/L $Pt(NO_3)_2$ solution was added dropwise under sonication and held for 10 min. All galvanic replacement operations were performed with no exposure of the catalyst to air. The catalyst was filtered, washed three times with 10 mL of distilled water, and dried at 60 °C under vacuum overnight. Pt–M_A SAAs (M= Cu, Fe, Co, Ni, Zn, Ga, Ag, Sn) and Pt–M_BCu SAAs (M_B= Zn, Ga, Sn) were also prepared in a same procedure.

The Pt and base metal (Cu, Fe) contents of each catalyst were analyzed by ICP (PS7800, Hitachi High-Tech Science Corporation) according to our previous study.[1]

1.2.2. Supported Pt, Cu, Fe, PtFeCu, and FeCu catalysts. A predetermined amount of 10 g/L $M(NO_3)_x$ aqueous solutions, r-TiO_2, and 50 mL of distilled water were added to a flask that can be attached to an evaporator and stirred at room temperature for 1h. The flask was attached to an evaporator and stirred in a water bath at 80°C, vacuum degassed, and the solution was evaporated to dryness. Subsequently, the catalyst was dried overnight at 80 °C and calcined at 500°C for 1 h at an increase rate of 10 °C/min under the air. The resulting catalyst was reduced with H_2 gas at 300°C and used for experiments.

1.3. Activity tests.

The catalyst was pressed at 10 MPa for 10 s and sieved through a mesh with a size of 300–600 μm. A quartz U-tube (outer diameter, 6 mm; inner diameter, 4 mm) was filled with 10 or 50 mg of catalyst. The position of the catalyst was fixed with quartz wools. The quartz U-tube was attached to a gas-line. First, Ar gas was introduced into the tube to remove the air. After that, a pure H_2 gas was introduced. The temperature was then raised to 300 °C at a rate of 20 °C/min and kept for 1 h while flowing 100% H_2 gas at a rate of 20 mL/min. The H_2 supply was stopped and switched to Ar gas flow. After that, 1.6 % MCH/Ar gas mixture was introduced to the system. The 1.6 % MCH/Ar gas mixture was prepared upper stream by passing Ar gas through an MCH bubbler cooled to 0 °C. Concentrations of MCH and TOL in the outlet gas were analyzed by gas chromatograph (SHIMADZU GC 2030N) equipped with a barrier discharge ionization detector connected to RT-Msieve 5A and RtÒ-Q-BOND capillary columns. Arrhenius plots were obtained based on the activity tests at 320, 310, 300, 290, and 280 °C using the catalyst pretreated with H_2 at 320 °C for 1 h. All kinetic experiments were performed under 1.6% MCH/20% H_2/Ar gas mixture. The validity of the procedure has been verified in our previous work.[2]

The definition of each catalytic performance is as follows:

$$\text{MCH conversion (\%)} = \frac{\text{TOL concentration (\%)}}{\text{MCH concentration (\%)} + \text{TOL concentration (\%)}} \times 100$$

$$\text{TOL selectivity (\%)} = \frac{\text{TOL concentration (\%)}}{\text{TOL concentration (\%)} + \text{CH}_4\text{ concentration (\%)}} \times 100$$

$$\text{H}_2\text{ evolution rate } (\text{mmol}_{\text{H}_2}/\text{g}_{\text{Pt}}/\text{min}) = \frac{3 \times \text{MCH conversion (\%)} \times \text{MCH feeding rate (mmol/min)}}{100 \times \text{mass of Pt used in activity test } (\text{g}_{\text{Pt}})}$$

Here, the "mass of Pt used in activity test" was determined based on the ICP and catalyst loading used in the activity test. In the manuscript, TOF is also given. Please note that this term is responsible for the H_2 evolution rate normalized with "mole of Pt (mol_{Pt})" instead of the "mass of Pt (g_{Pt})" to at the above definition, where the "mole of Pt (mol_{Pt})" means the total number of Pt present at the catalyst (*not "mole of surface Pt"*). Since the amount of the Pt single atoms is below the detection limit of the CO-pulse experiment due to the low content (<0.1 wt%), the fraction of surface Pt atoms cannot be estimated. Furthermore, in this case, Cu and Fe are also active for CO adsorption (refer to **Fig. 5**); therefore, we cannot selectively titrate surface Pt only. Therefore, TOF was calculated based on the total mole of Pt. If the part of the Pt single atoms was diffused into the bulk of the supported Fe/Cu, the accurate TOF would be higher than the value described in the manuscript.

Since all catalysts showed TOL selectivity of more than 99.8% upon the activity tests, activity and durability are mainly discussed in the manuscript. The data concerning TOL selectivity were given only for the best catalyst (Pt–FeCu SAA).

1.4. Characterization.

1.4.1. Synchrotron-based PXRD. The catalyst was loaded into a quartz capillary (Hilgenberg; outer diameter, 0.7 mm; wall thickness, 0.01 mm) and attached to an in-situ cell holder at a BL5S2 of an Aichi Synchrotron Radiation Center (Aichi SR). This in-situ cell holder was connected to a gas line that allows us to vacuum the air in the capillary and introduce the H_2 gas into the capillary. The air within the capillary was first evacuated at room temperature. After that, 0.1 MPa of 100% H_2 was introduced into the capillary. Under 0.1 MPa H_2, the catalyst was heated to 300 °C at an increase rate of 10 °C/min and maintained for 1 h for the reduction. After that, XRD profiles were acquired under 0.1 MPa H_2 at 300 °C with a PILATUS100K detector and monochromatic beam (λ= 0.69962 Å) at BL5S2 of Aichi SR.

1.4.2. XAFS spectroscopy. The catalyst was formed into a 10Φ pellet, placed in an in-situ transmission/fluorescence XAFS cell made of quartz. The position of the pellet was fixed by the inner quartz tube with a slit. The in situ XAFS cell was connected to a gas-line that allows us to supply He and H_2 into the cell. First, the air in the cell was removed by He flow and then purged with a pure H_2 gas with a flow rate of 20 mL/min. Under the flow of H_2, the catalyst was heated up to 300 °C with an increase rate of 20 °C/min for the reduction. Temperatures were measured with a thermocouple inserted in cells near the catalyst location. After cooling down to 50°C, XAFS measurements were performed at the Pt L_{III} or Fe/Cu K-edge. The Pt L_{III} edge XAFS spectrum was acquired by the fluorescence method at BL5S1 (Aichi SR), whereas the Fe/Cu K-edge by the transmission method at BL11S2 (Aichi SR). Ionization chambers and a seven-element silicon drift detector (SDD) were used. For the fluorescence mode, aluminum foil was placed in front of the SDD to reduce the X-ray fluorescence emitted from the r-TiO_2 support as much as possible. In each measurement, a metallic foil of the target element was measured simultaneously, and the energy in the obtained spectrum was calibrated.

Using Athena and Artemis software with FEFF6.0 included in the Demeter package,[3] XANES and EXAFS spectra were processed and analyzed. The WT was carried out with software developed by ESRF[4-5] and Morlet wavelet. WT parameters of κ= 15 and σ= 1 were used for the WT of Pt L_{III}-edge EXAFS function weighted with k^3 in a range of $3 < k < 12$ Å^{-1}. On the other hand, WT parameters of κ= 7 and σ= 1 were used for the WT of Fe K-edge EXAFS function weighted with k^2 in a range of $3 < k < 11$ Å^{-1}.

1.4.3. CO-FTIR spectroscopy. 10 mg of catalyst was formed into a pellet of 10 Φ in diameter. The disk was set in an in situ FTIR cell made of quartz. Then the pellet was fixed by the inner quartz tube with slit. The in situ cell was connected to a gas line that allows us to supply Ar, H_2, and CO. After removal of the air in the cell by purging with Ar, the catalyst was exposed to H_2 at a flow rate of 20 mL/min. The temperature was raised to 300 °C at an increase rate of 10 °C/min and kept for 1 h. The temperatures were measured by a thermocouple near the position of the catalyst. After the reduction, the H_2 flow was switched to Ar flow and the temperature was cooled to 50°C. After the stabilization of the temperature, the background spectrum was collected. Next, 0.1% CO/Ar gas mixture was introduced into the cell with a flow rate of 50 mL/min for 30 min. After that, the 0.1% CO/Ar gas mixture was

switched to Ar. The stabilization time was 30 min. The CO-FTIR spectrum was then collected with a transmission mode using a JASCO FT/IR-6600 spectrometry equipped with a mercury cadmium telluride detector. The measurement range was 4000−600 cm^{-1}, the resolution was 2 cm^{-1}, and the number of integrations was 64.

1.4.4. HAADF-STEM and in-situ TEM. The catalyst was calcined at 300 °C at an increase rate of 10 °C/min under 100% H_2 flow (20 mL/min) and kept for 1 h. A small amount of the pretreated catalyst and 3 mL of distilled water were added to the sample bottle. This was sonicated for 30 min to disperse the catalyst. Distilled water in which the catalyst was dispersed was collected with a Pasteur pipette and deposited on a 200-mesh lacey carbon-coated Cu or Mo grid (EM Japan Co., Ltd.). The grid was vacuum-dried overnight in a desiccator and used for observation. A JEM-ARM200F Cold/Thermal (JEOL) with an acceleration voltage of 200 kV was used for HAADF-STEM observation.

In situ TEM observation was performed using a JEM-1000K RS (JEOL Ltd.) with the acceleration voltage of 1000 kV. The 200-mesh lacey carbon-coated Cu or Mo grid (EM Japan Co., Ltd.) with the catalyst was transferred to the measurement room. The 20% H_2/N_2 gas was introduced into the measurement room. The pressure was controlled to be 6 mbar by simultaneous evacuation at the downstream. Temperature was then raised to 300 °C at 10 °C/min under the gas flow and kept for 1 h. After the pretreatment, the catalyst was cooled to room temperature and the gas supply was stopped for 15 min. All pre-treatments were performed in a measurement room of a JEM-1000K RS for in situ measurements with no exposure of the catalyst to air. The average particle size was determined by counting 206 particles using analysis software (Gatan Microscopy Suite ver 3.43.3213.0 AMTEK).

1.4.5. XPS. The atomic molar ratio of Fe and Cu were estimated by XPS on the reduced catalyst. The XPS measurement was performed at room temperature on the catalysts after the pre-treatments with H_2. PHI Quantes (ULAVAC-PHI; source: Al Kα) was used. The energy step size was 0.05 eV and Dwell time was 20 ms. Based on the peak intensities of Cu-$2p_{3/2}$ and Fe-$2p_{3/2}$ signals and element-specific sensitivity coefficients, the surface atomic molar ratio was calculated with PHI Elite (ULAVAC-PHI). Note that our experimental environment does not allow us to measure XPS with the catalyst completely non-exposed to the atmosphere; thus, true electronic

structures of the surface Cu and Fe cannot be discussed based on the XPS data.

1.4.6. In situ Raman spectroscopy. Raman spectra were measured using a JASCO RMP-330 spectrophotometer equipped with a 532 nm green semiconductor laser as an excitation source. The catalyst was placed in an in situ diffuse reflectance cell having a quartz window (15 mm) and an internal heating system connected to a gas flow system. A 20× objective optical lens was used to focus the depolarized laser beam on the sample surface and to collect the backscattered light. The backscattered light was dispersed by a single-stage spectrometer with 1800-groove mm^{-1} grating and acquired by an air-cooled 1024×256 pixel charge-coupled device. First, the catalyst was exposed to the H_2 gas 300 °C. The Raman spectra were collected under the 1.6% MCH/Ar gas mixture with a resolution of 1 cm^{-1}. The exposure time was 15 s and 3 scans were accumulated for each spectrum.

1.4.7. TOL breakthrough curve. The catalyst was pressed at 10 MPa for 10 s and sieved through 300–600 mesh. A quartz U-tube (outer diameter, 6 mm; inner diameter, 4 mm) were filled with 50 mg of catalyst. The position of the catalyst was fixed with quartz wool. The quartz U-tube was attached to a gas-line that allows us to supply Ar, H_2, and TOL. First, Ar gas was introduced into the tube to remove the air. After that, a pure H_2 gas was introduced. The temperature was then raised to 300 °C at a rate of 20 °C/min and kept for 1 h while flowing H_2 at a rate of 20 mL/min. Next, the H_2 gas was switched to Ar and cooled to 50°C. After the temperature stabilized, the 0.8 % TOL/Ar gas was introduced into the system by passing the Ar gas through the MCH bubbler cooled to 0°C. The outlet TOL concentration was monitored by FT-IR with a triglycine sulfate detector (Shimadzu, IRSpirit). The gas cell with two KRS-5 windows was used to analyze the gas-phase TOL, which was attached directly to the downstream of the gas line. An optical path length in the gas cell was 10 cm. The intensity of the IR band at 729 cm^{-1} for TOL was used as the spectroscopic probe to quantify the TOL concentration. A calibration curve was prepared in advance and used for the quantitation. The measurement conditions are as follows: measurement range, 4000−600 cm^{-1}; resolution, 8 cm^{-1}; number of integrations, 1.

1.4.8. TPO. 50 mg of catalyst was placed in a quartz tube and attached to a measurement apparatus (BELCAT II). The catalyst was heated to 300 °C with an increase rate of 20 °C/min under H_2 flow with a flow rate of 20

mL/min and held for 1 h. Temperature was measured with a thermocouple inserted in the quartz tube. The position of the thermocouple was near the catalyst. To deposit coke on the catalyst surface, the gas was switched to a 1.6% MCH/Ar gas mixture and the catalyst was heated at 500 °C for 12 h. The MCH/Ar gas mixture was prepared at the upper stream by passing the Ar gas through an MCH bubbler. The temperature was then cooled to 50 °C. The gas was switched to Ar to remove MCH in the quartz tube. A 20% O_2/He gas mixture was then introduced into the quartz tube at a flow rate of 20 mL/min for TPO measurement. The measurement temperature was set to 50–900°C. The rate of temperature increase was 10°C/min. The mass signal of carbon dioxide (m/z= 44) produced by coke combustion was traced by on-line mass spectroscopy (BEL MASS, MicrotracBEL) attached directly to the downstream of the instrument.

1.4.9. MCH-TPR 50 mg of catalyst was placed in a quartz tube and attached to a measurement apparatus (BELCAT II). Pretreatment conditions were the same as for the TPO measurement. After pretreatment, the temperature was lowered to 50°C and the activated catalyst was exposed to a 1.6% MCH/ Ar gas mixture at a flow rate of 20 mL/min. Under these gas flow conditions, MCH-TPR was performed at 50–900°C. The mass signal of H_2 (m/z= 2) produced in the MCH dehydrogenation reaction was monitored by an on-line mass spectroscopy (BEL MASS, MicrotracBEL) attached directly to the downstream of the instrument.

1.5. DFT calculation.

The geometrical optimizations were conducted using spin-polarized periodic DFT calculations. The Vienna ab initio simulation package was used,[6-9] employing the projector augmented wave method[10-11] and the generalized gradient approximated Perdew−Becke−Ernzerhof exchange-correlation functional.[12-13] The van der Waals interactions were included by applying the Becke−Johnson damping dispersion correction.[14-15] Gaussian smearing with a width of 0.05 eV was applied. Slab models of the most stable facet of Fe(110) with 15 Å of vacuum spacing were designed based on the pre-optimized bcc crystal structure of Fe. The unit cell of the designed slab model was (4 × 4). The Pt single atoms alloyed bcc-Fe(110) surfaces were modeled by replacement of two surface Fe atoms of the bcc-Fe(110) slab model with two Pt atoms. Using a *k*-points mesh with a spacing of 0.02 /Å, the reciprocal space was sampled. An energy cutoff of 520 eV was used for the plane-wave basis. The convergence criteria of the self-consistent field

electronic energies and the atomic forces were set to 10^{-6} eV and 0.02 eV/Å, respectively. The Fe atoms in the lowest layer were fixed in the structural optimizations. The structures were depicted using VESTA software.[16]

2. Supporting data

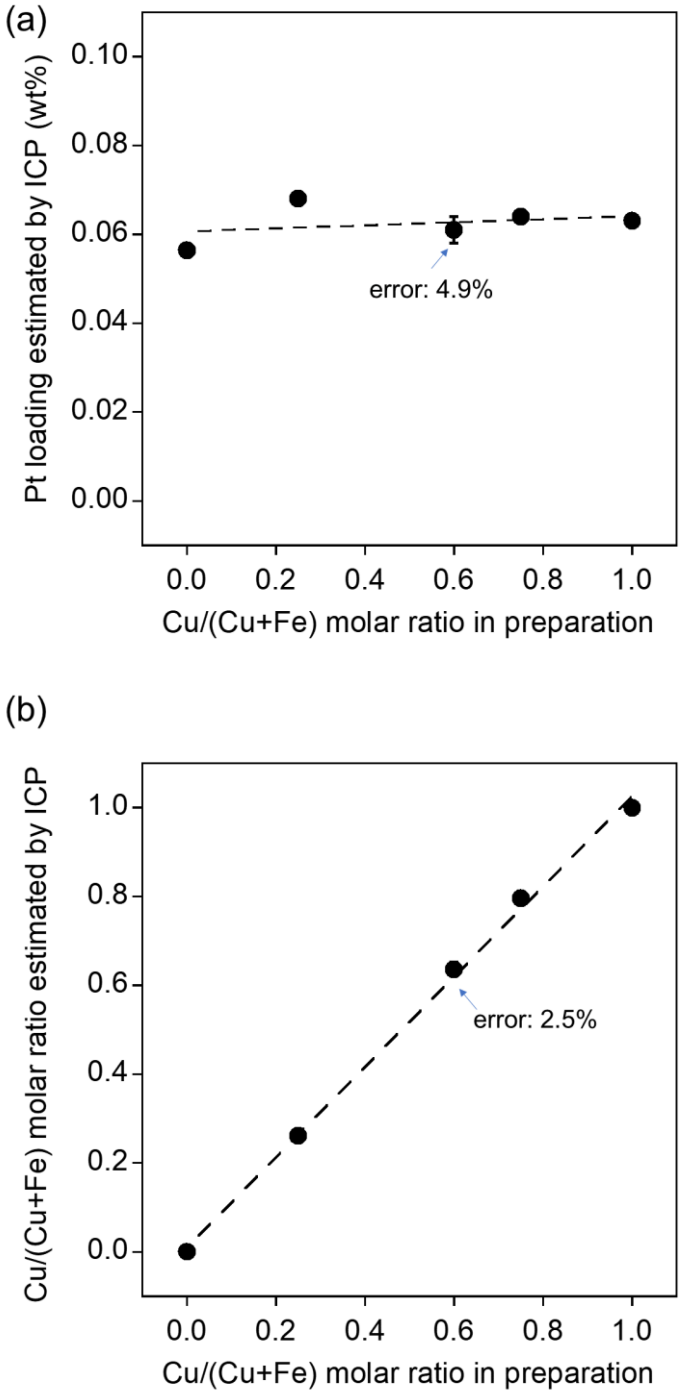

Fig. S1 (a) Pt loading and (b) Cu/(Cu+Fe) molar ratio determined by ICP. These are plotted against Cu/(Cu+Fe) molar ratios in the catalyst preparations.

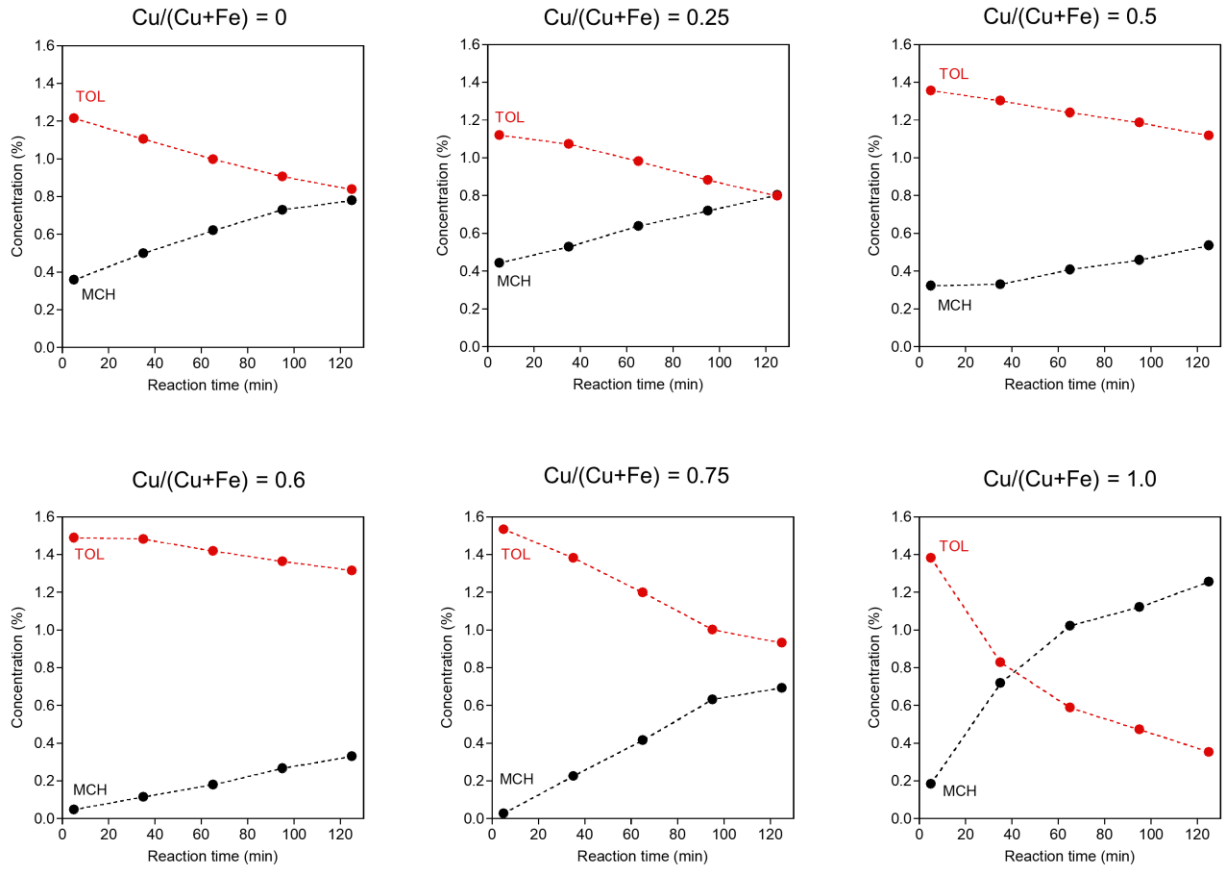

Fig. S2 Time courses of concentrations of TOL and MCH during the reaction over Pt–FeCu SAA catalysts. Reaction conditions: feed gas, 1.6% MCH (Ar, balance) with a flow rate of 20 mL/min; reaction temperature, 300°C; catalyst amount, 50 mg.

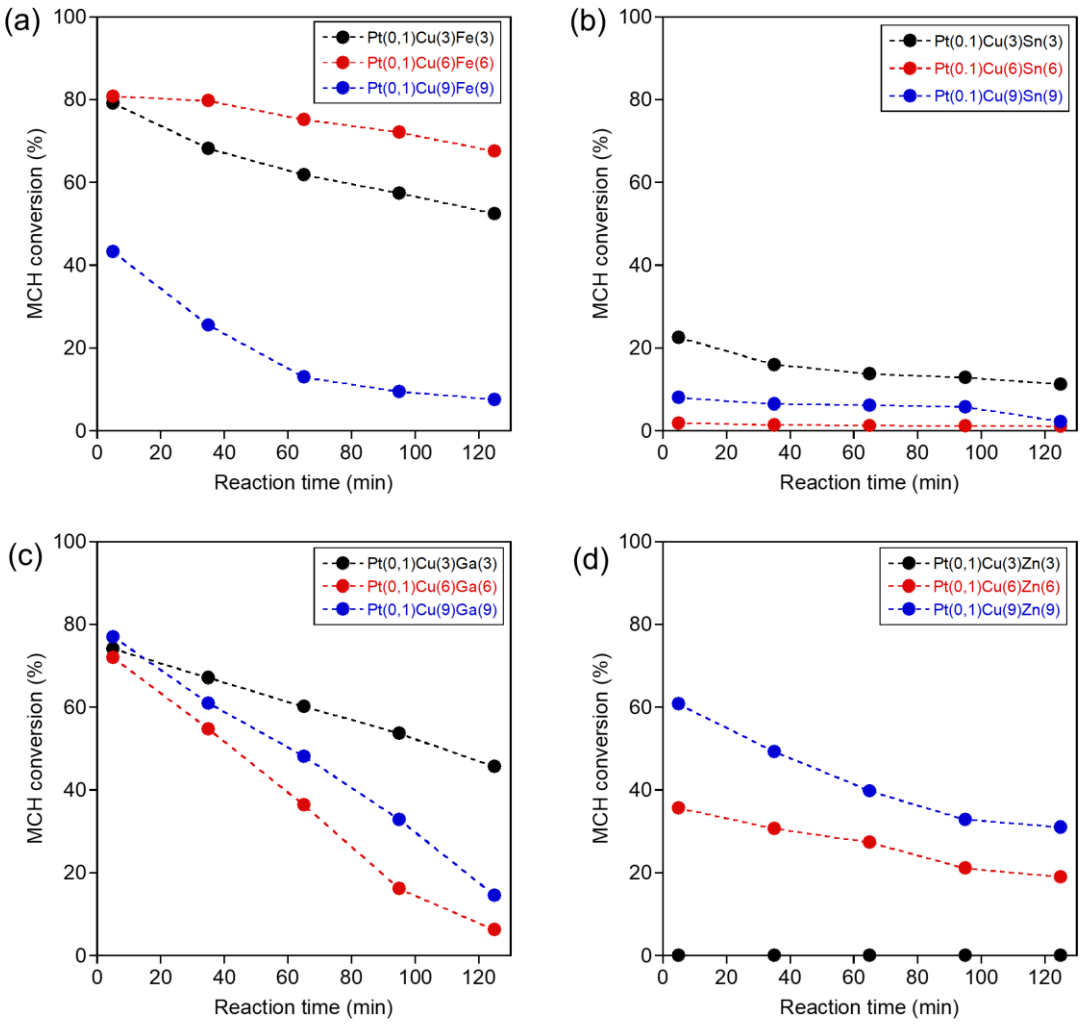

Fig. S3 Activity of Pt–CuM_B SAA catalysts: M_B= (a) Fe, (b) Sn, (c) Ga, (d) Zn. Loadings of Cu and M_B in the impregnation processes were set to 3, 6, or 9 wt%. Pt loading was 0.1 wt%. Reaction conditions: feed gas, 1.6% MCH (Ar, balance) with a flow rate of 20 mL/min; reaction temperature, 300°C; catalyst amount, 50 mg.

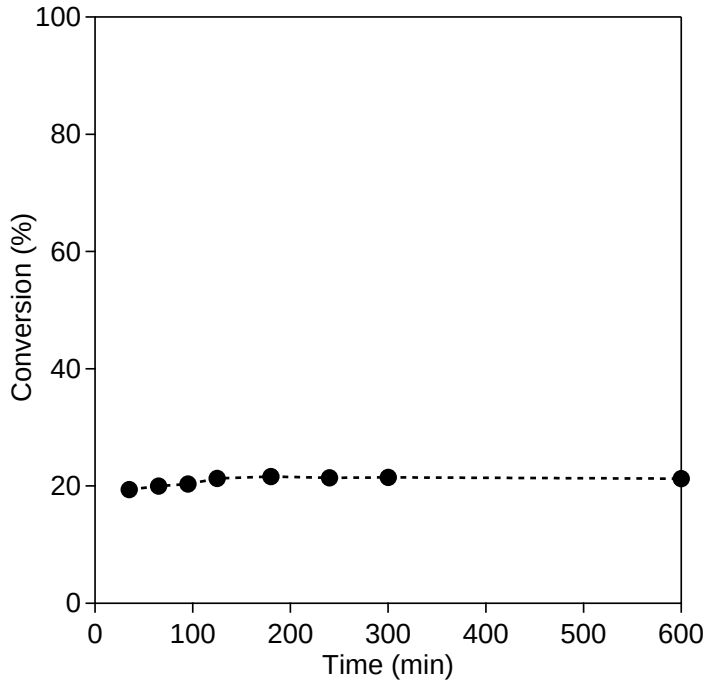

Fig. S4 MCH conversion in the durability test. Reaction conditions: feed gas, 1.6% MCH-20% H_2 (Ar, balance) with a flow rate of 20 mL/min; reaction temperature, 350°C; catalyst amount, 10 mg.

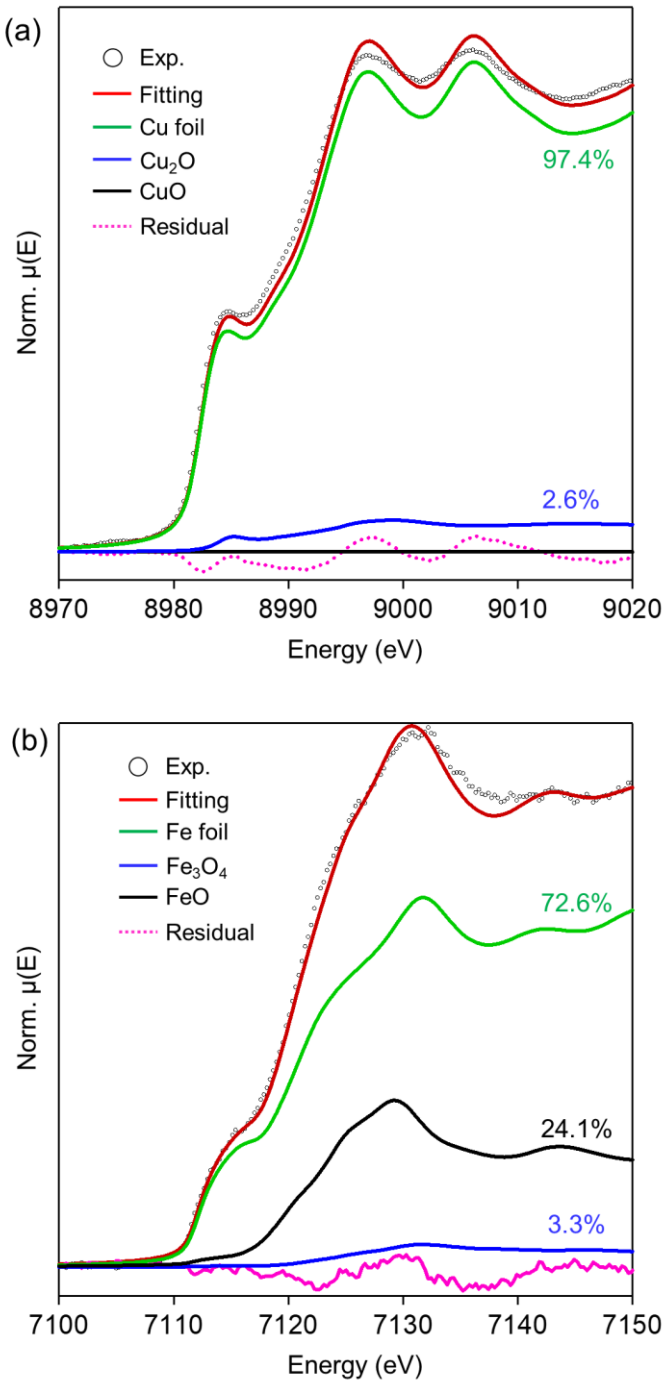

Fig. S5 LCF analysis of (a) Cu and (b) Fe K-edge XANES spectra of Pt–FeCu SAA.

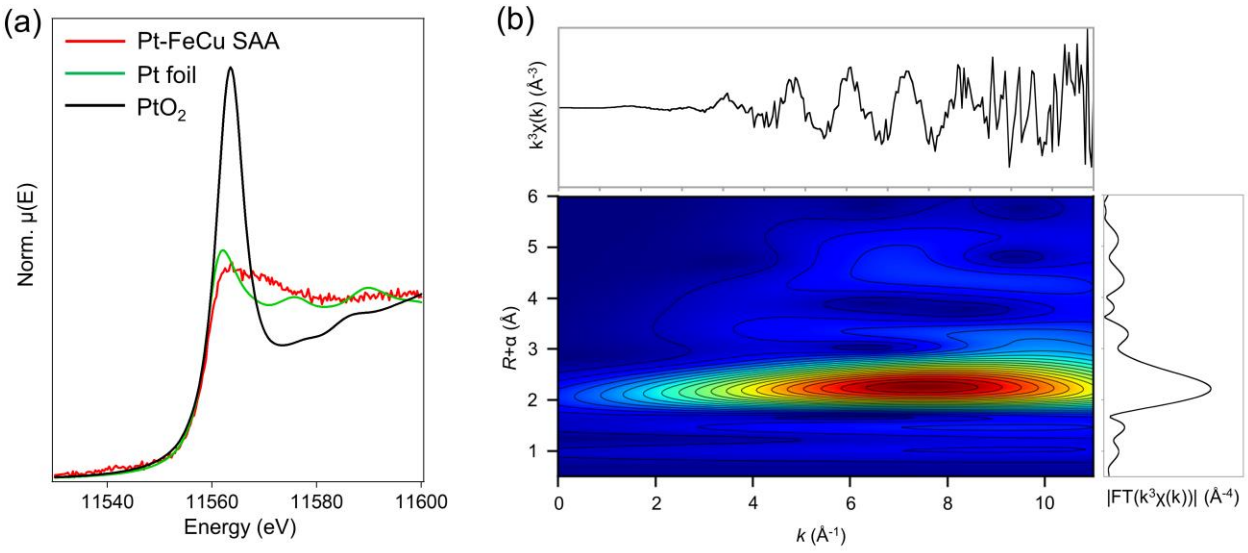

Fig. S6 WT-EXAFS of Pt–FeCu SAA after the activity test for 2 h in the absence of H_2.

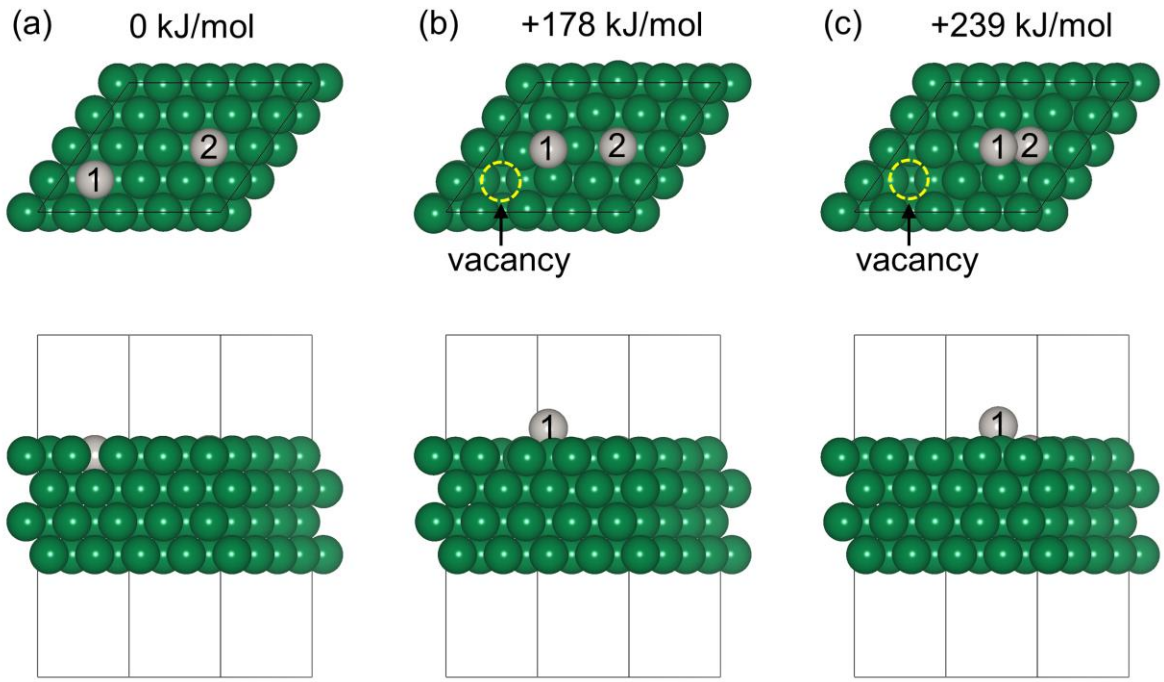

Fig. S7 Slab models of Pt–Fe SAA for representing the process of aggregation of Pt on bcc-Fe. Relative energy of the models is also given. Legend: green, Fe; gray, Pt.

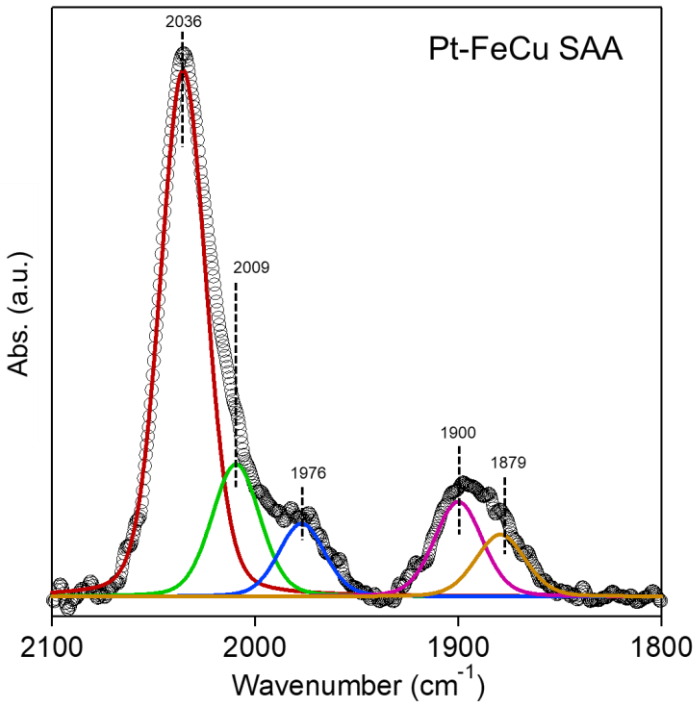

Fig. S8 The deconvolution analysis of CO-FTIR spectrum of Pt–FeCu SAA.

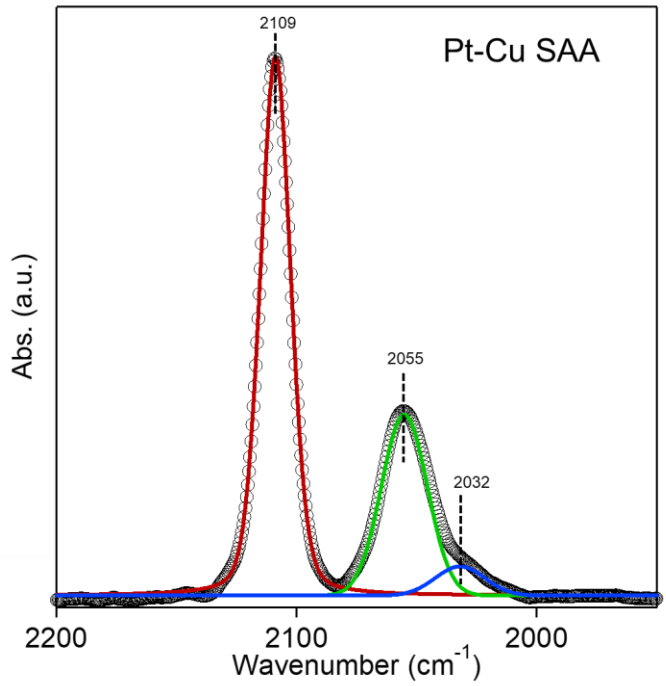

Fig. S9 The deconvolution analysis of CO-FTIR spectrum of Pt–Cu SAA.

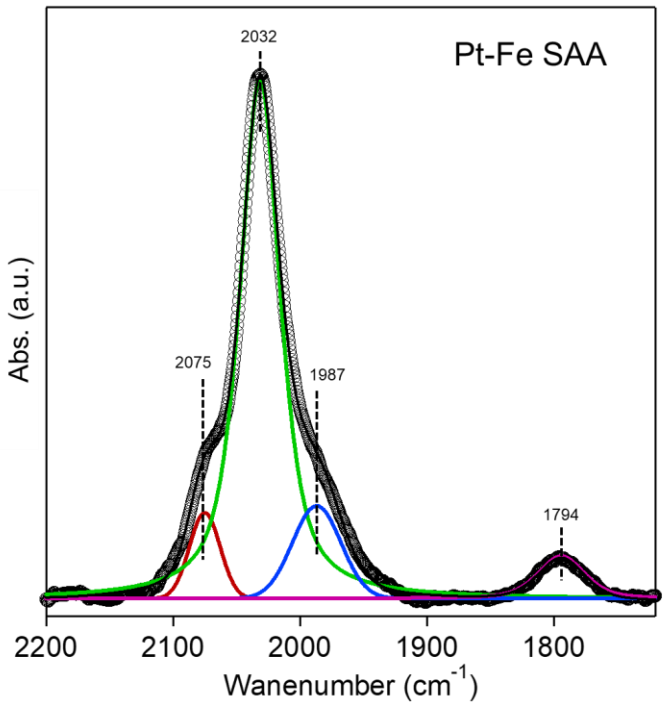

Fig. S10 The deconvolution analysis of CO-FTIR spectrum of Pt–Fe SAA.

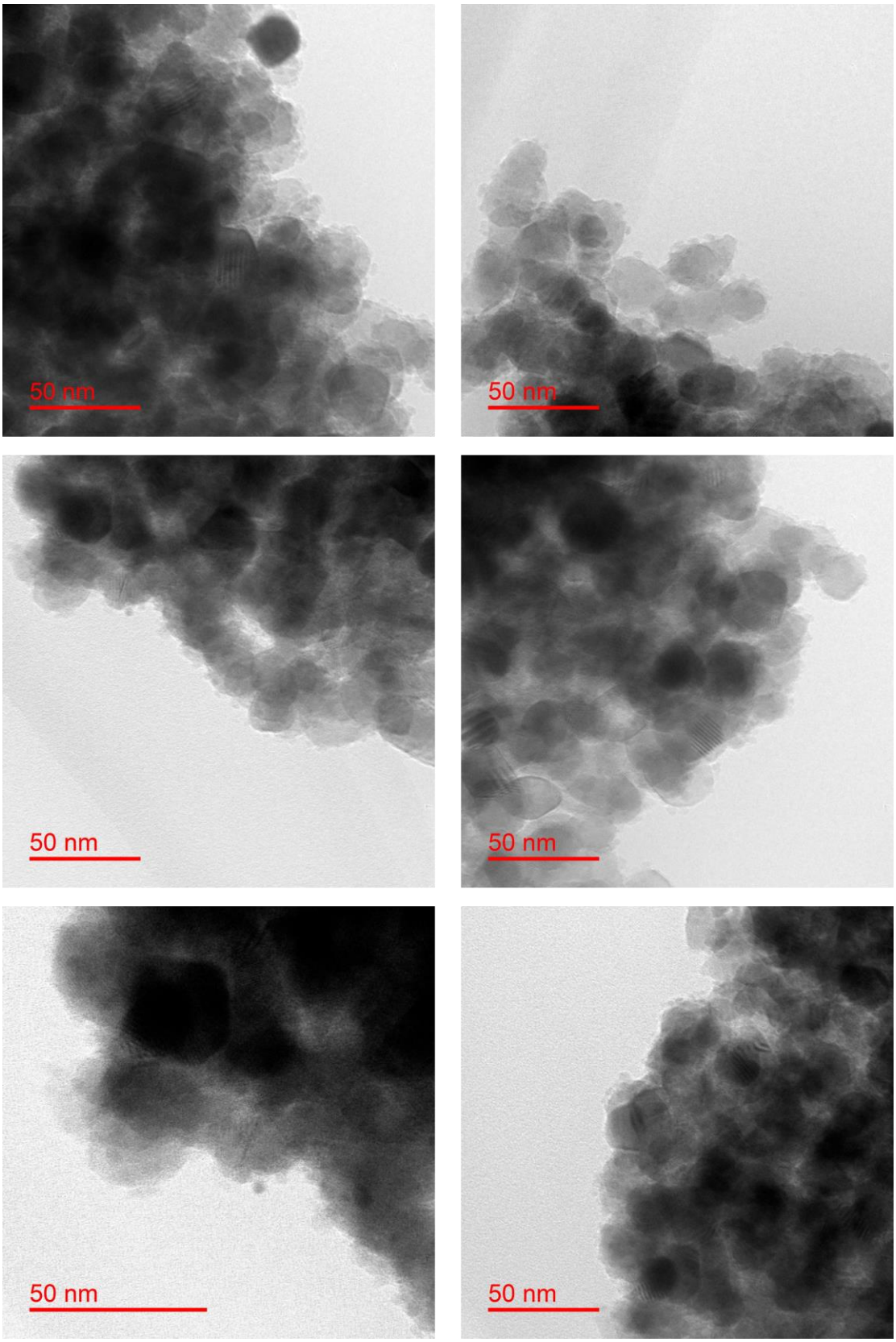

Fig. S11 Additional in situ TEM images of Pt–FeCu SAA.

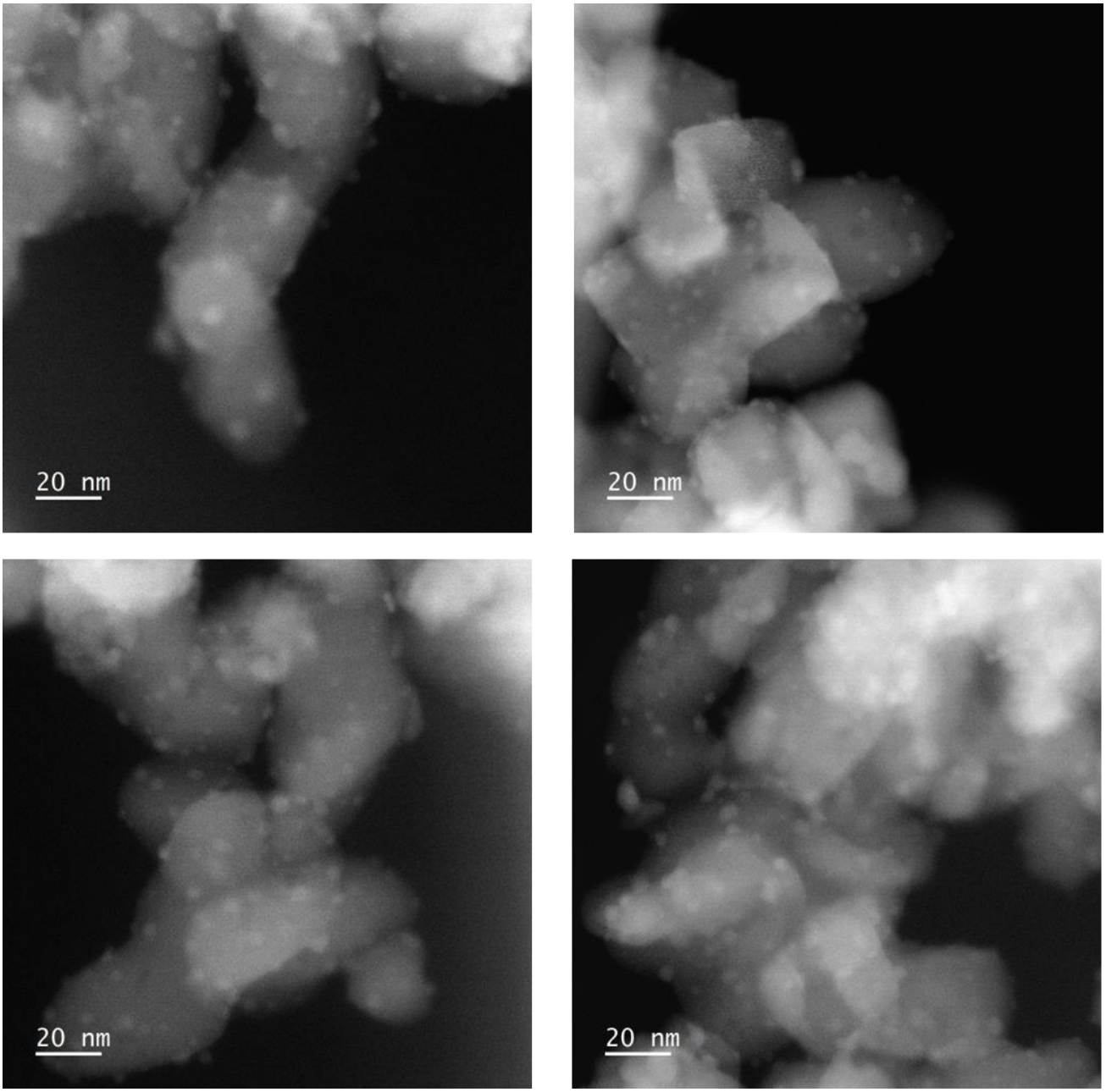

Fig. S12 Additional HAADF-STEM images of Pt–FeCu SAA with low magnification.

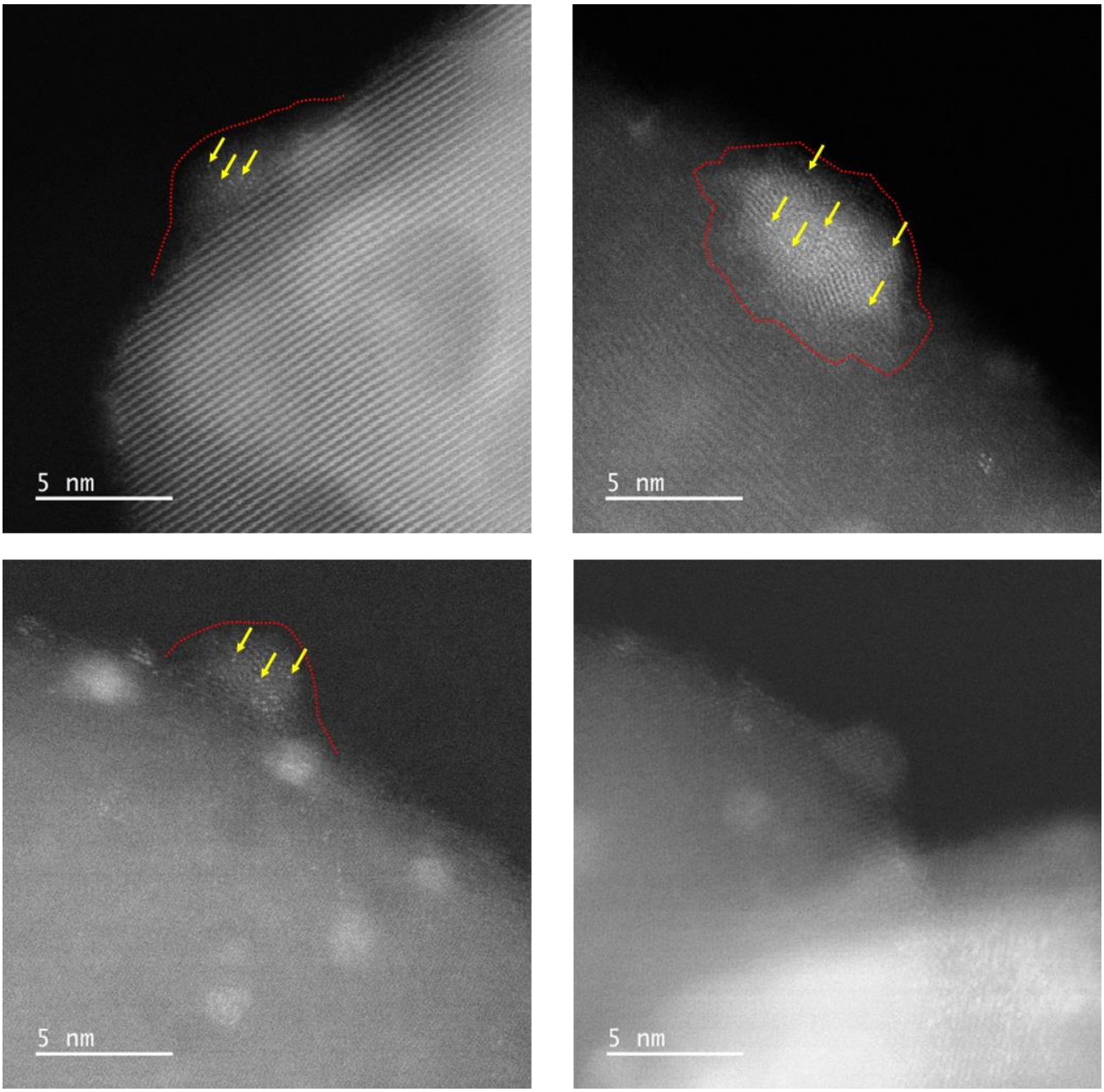

Fig. S13 Additional HAADF-STEM images of Pt–FeCu SAA with high magnification. Pt single atoms and Fe overlayer were highlighted by yellow arrows and a red dot line.

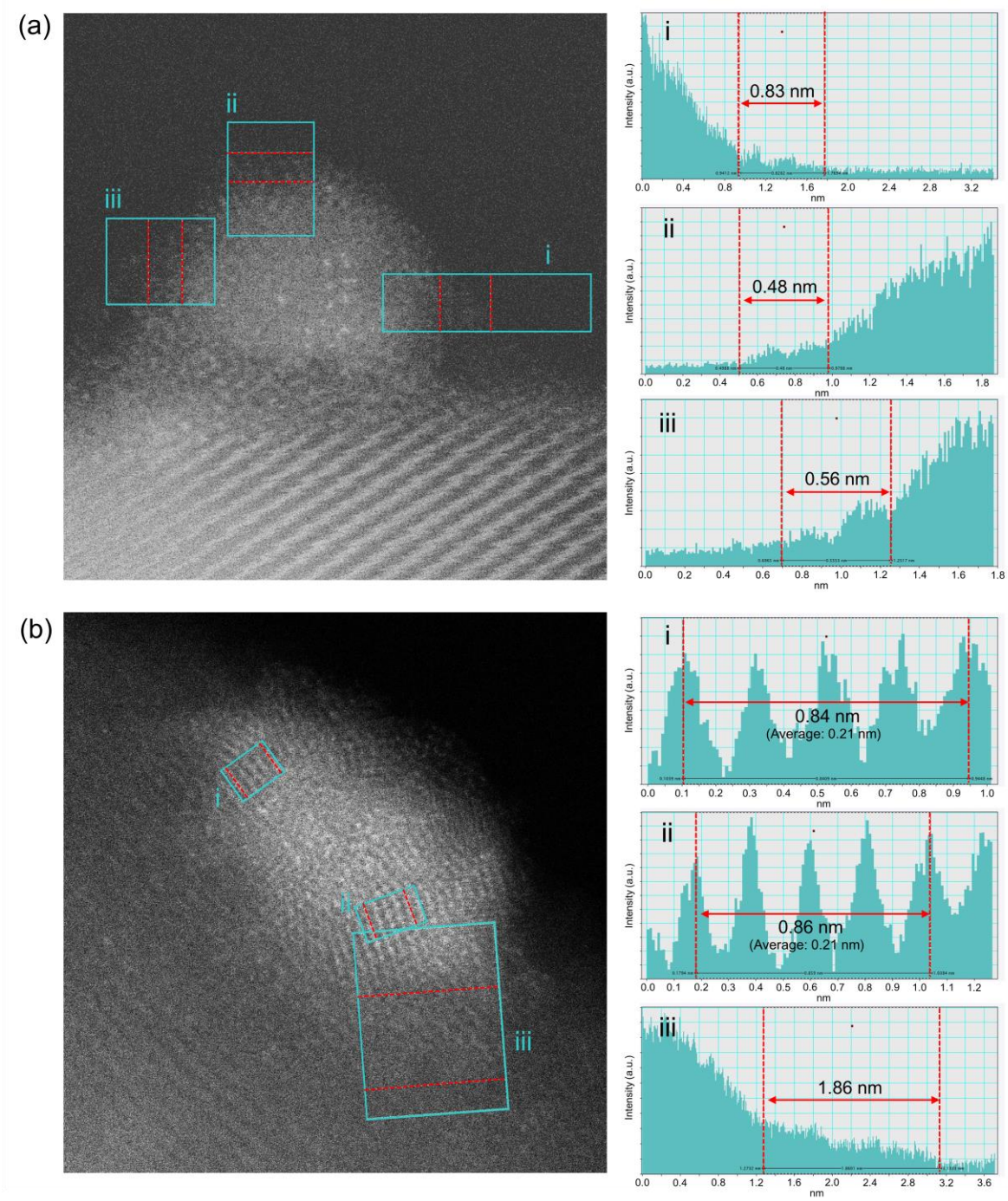

Fig. S14 Line scans of HAADF-STEM images of Pt–FeCu SAA with high magnification. For the image of (a), the thickness of the overlayer was measured. The line scans from the vacuum layer to the center of the particle revealed a region of gradual increase in intensity. This was defined as the overlayer region, and the thickness was measured. For the image (b), the lattice spacing of the nanoparticles was measured in the regions (i) and (ii). Furthermore, for demonstrating the presence of the layer structure spread onto the r-TiO_2, the region (iii) was also analyzed. The length between two red dot lines is given in the line scan profiles.

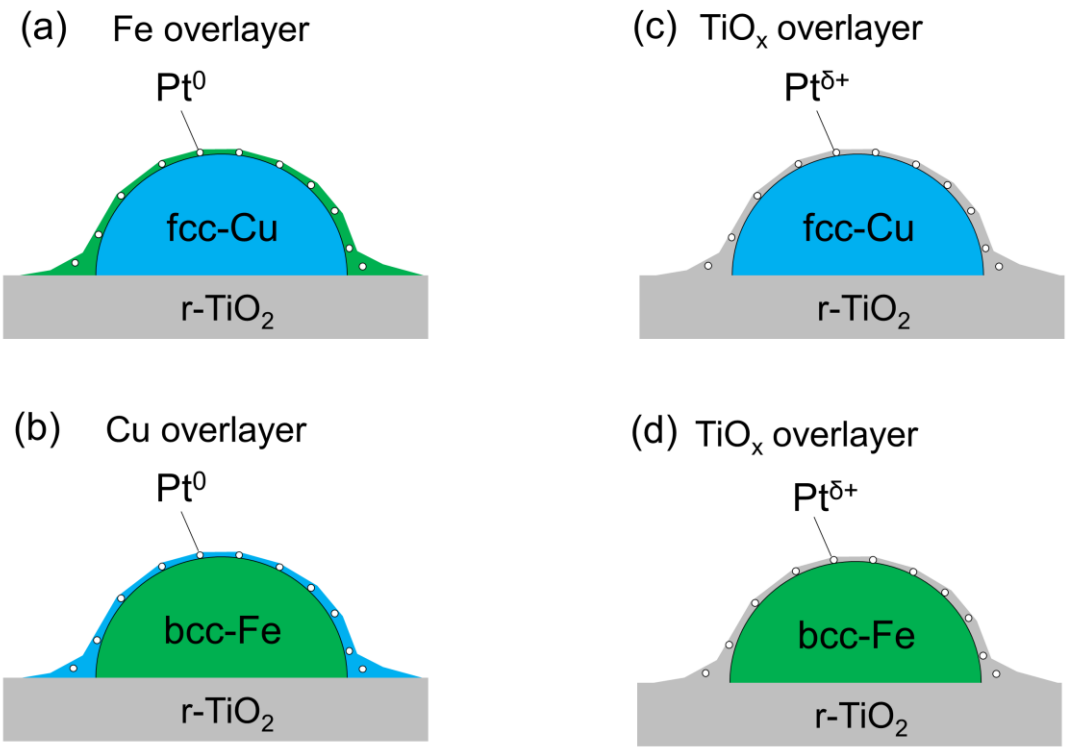

Fig. S15 Schemes of thin layers that can be formed in the present system.

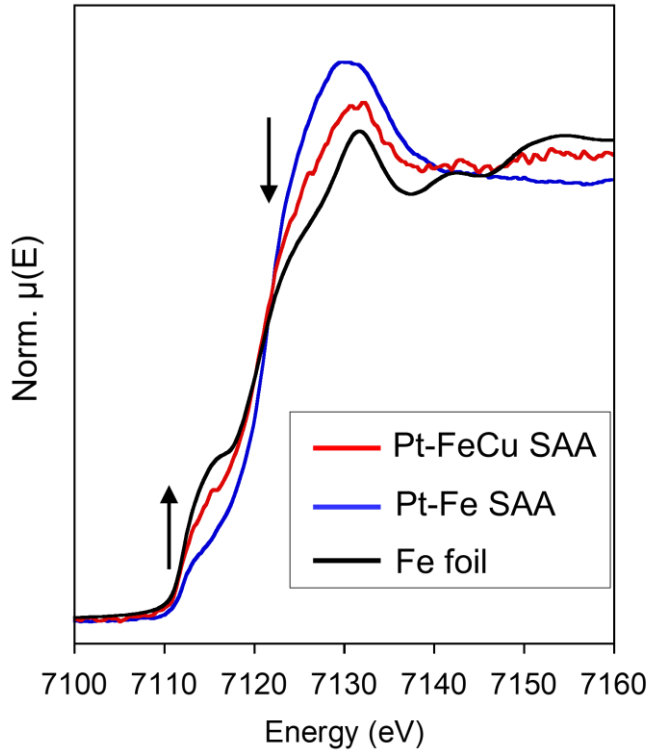

Fig. S16 Fe K-edge XANES spectra of Pt–FeCu SAA and Pt–Fe SAA. For comparison, datum of Fe foil is also given.

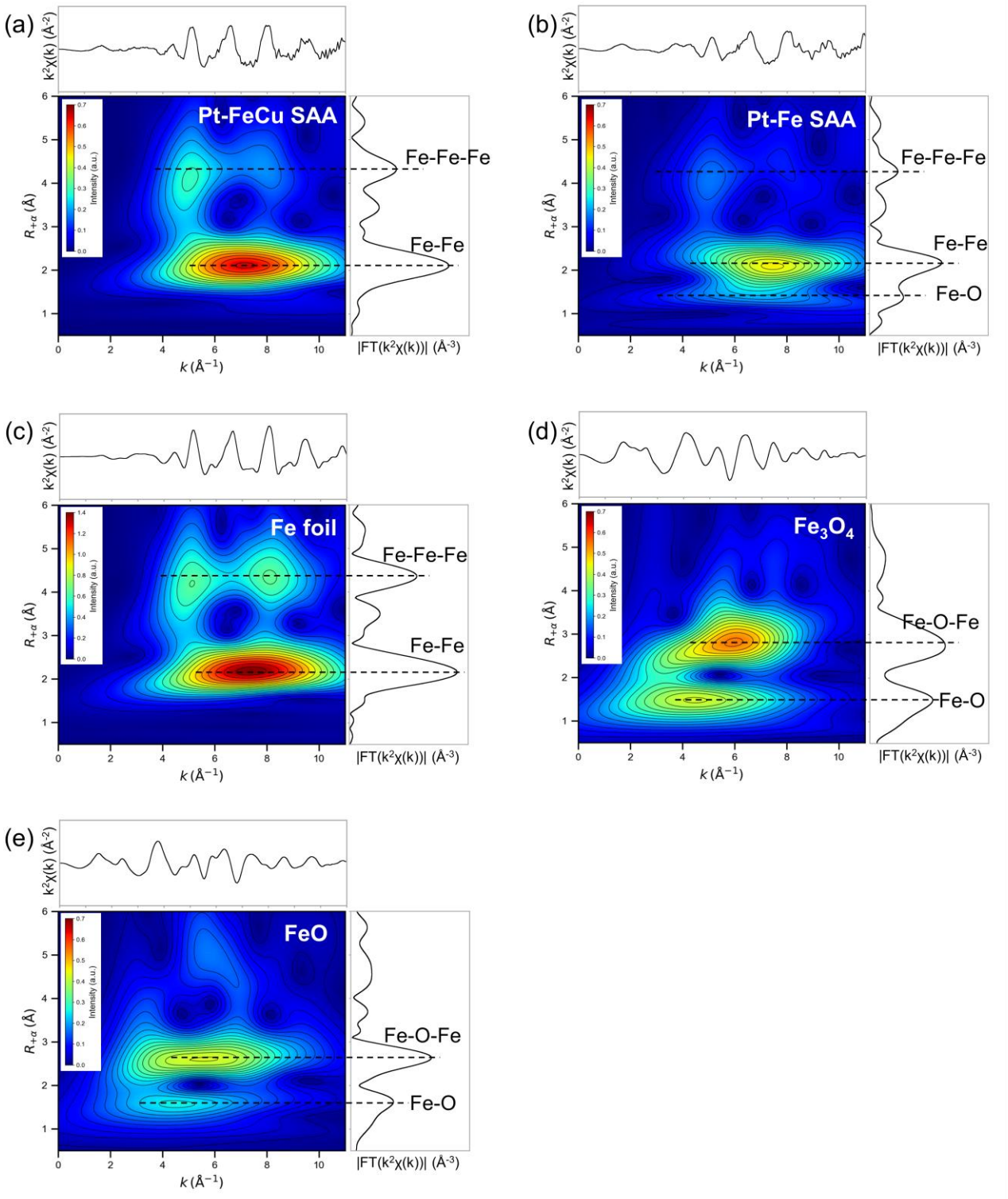

Fig. S17 (a-b) Fe K-edge WT-EXAFS of Pt–FeCu SAA and Pt–Fe SAA. (c-e) For comparison, data of reference materials are also given. The $k^2\chi(k)$ function in a range of $3 < k < 11$ Å^{-1} and Morlet wavelet with $\kappa = 7$, $\sigma = 1$ was used for the WT.

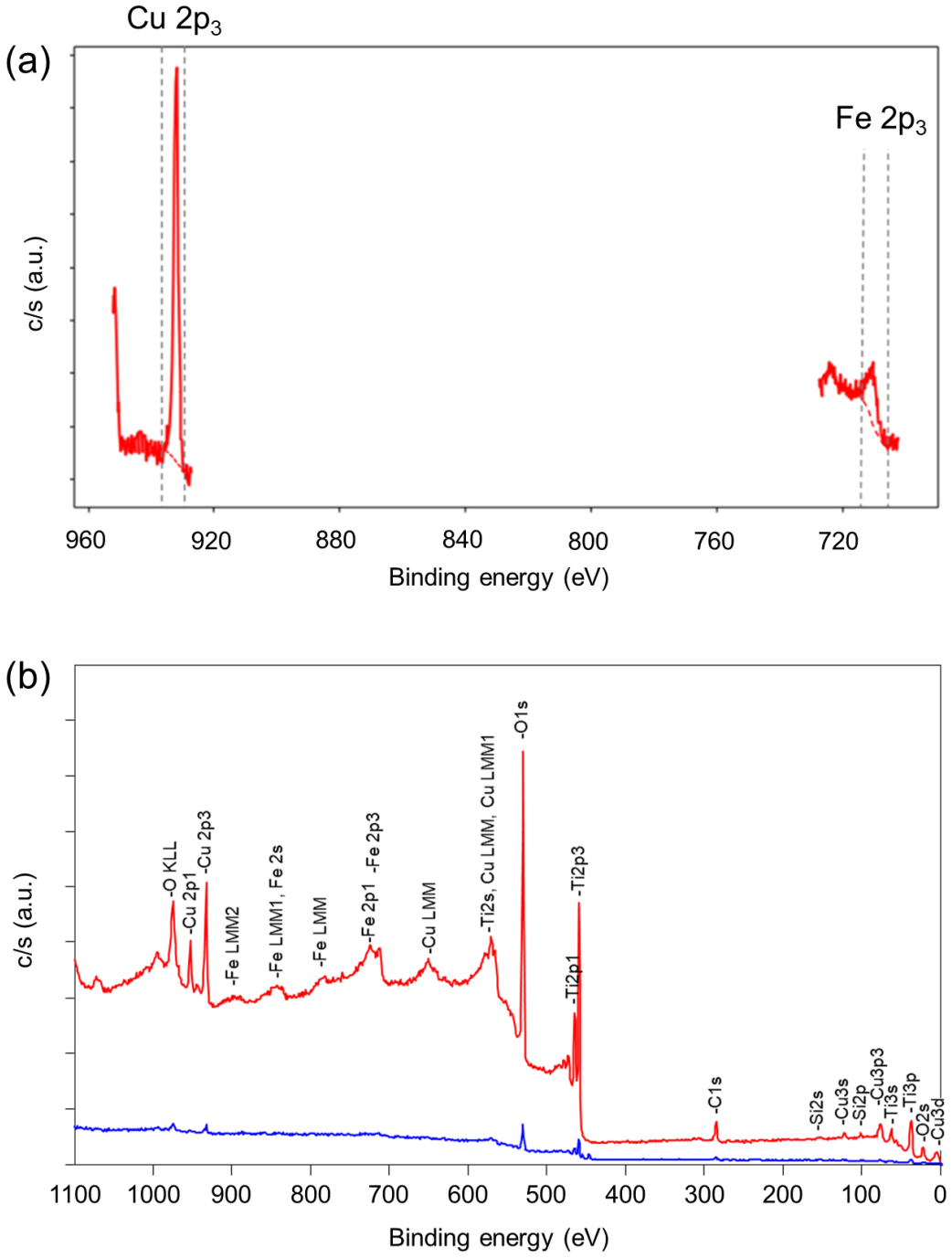

Fig. S18 (a) XPS-spectrum of Pt–FeCu SAA for calculation of surface atomic composition of Fe and Cu. (b) Whole spectrum.

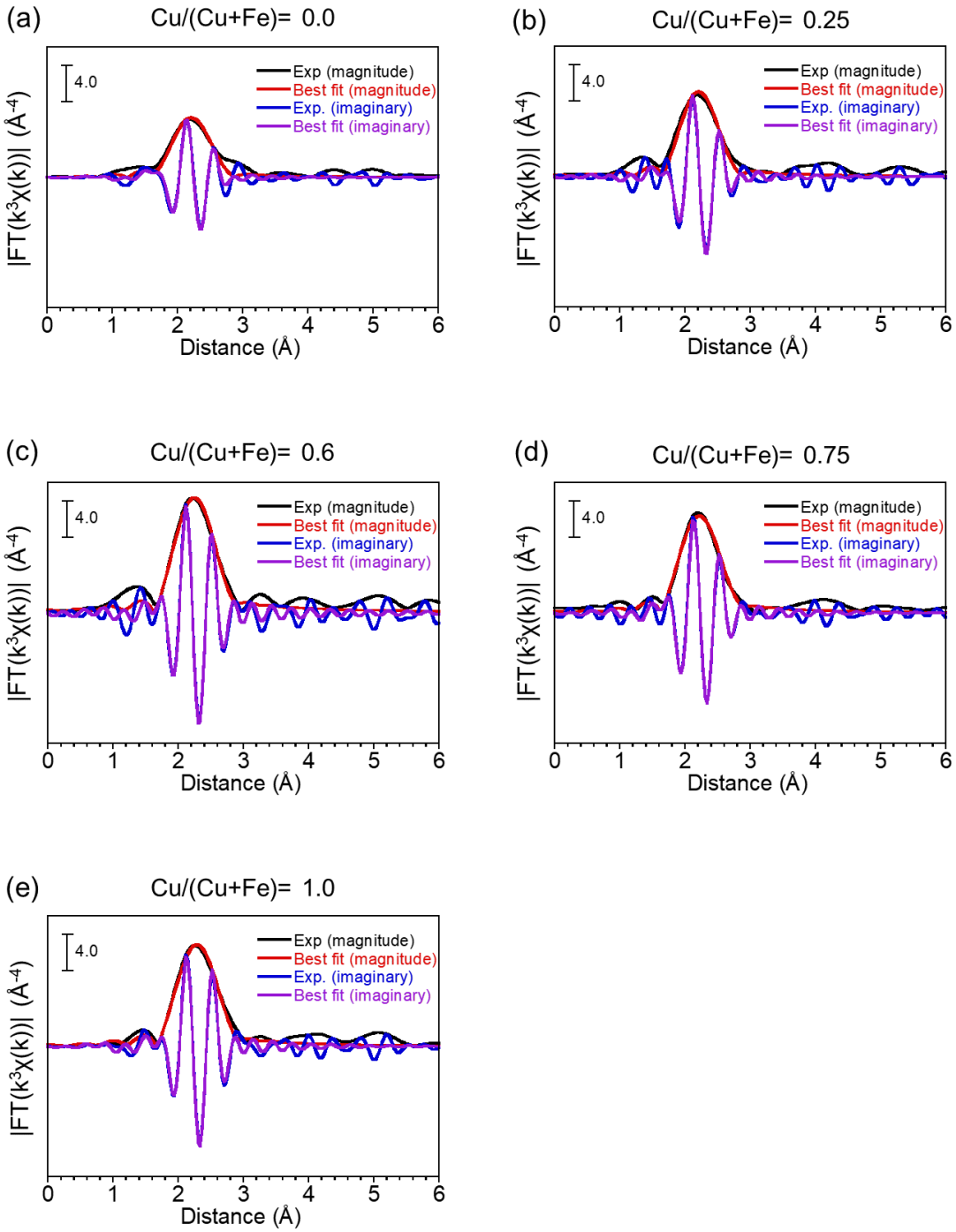

Fig. S19 Fitting details in a R-space for Pt L_{III}-edge EXAFS spectra of a series of Pt–FeCu SAAs with different Cu/(Cu+Fe) molar ratios: Cu(Cu+Fe)= (a) 0.0, (b) 0.25, (c) 0.6, (d) 0.75, (e) 1.0.

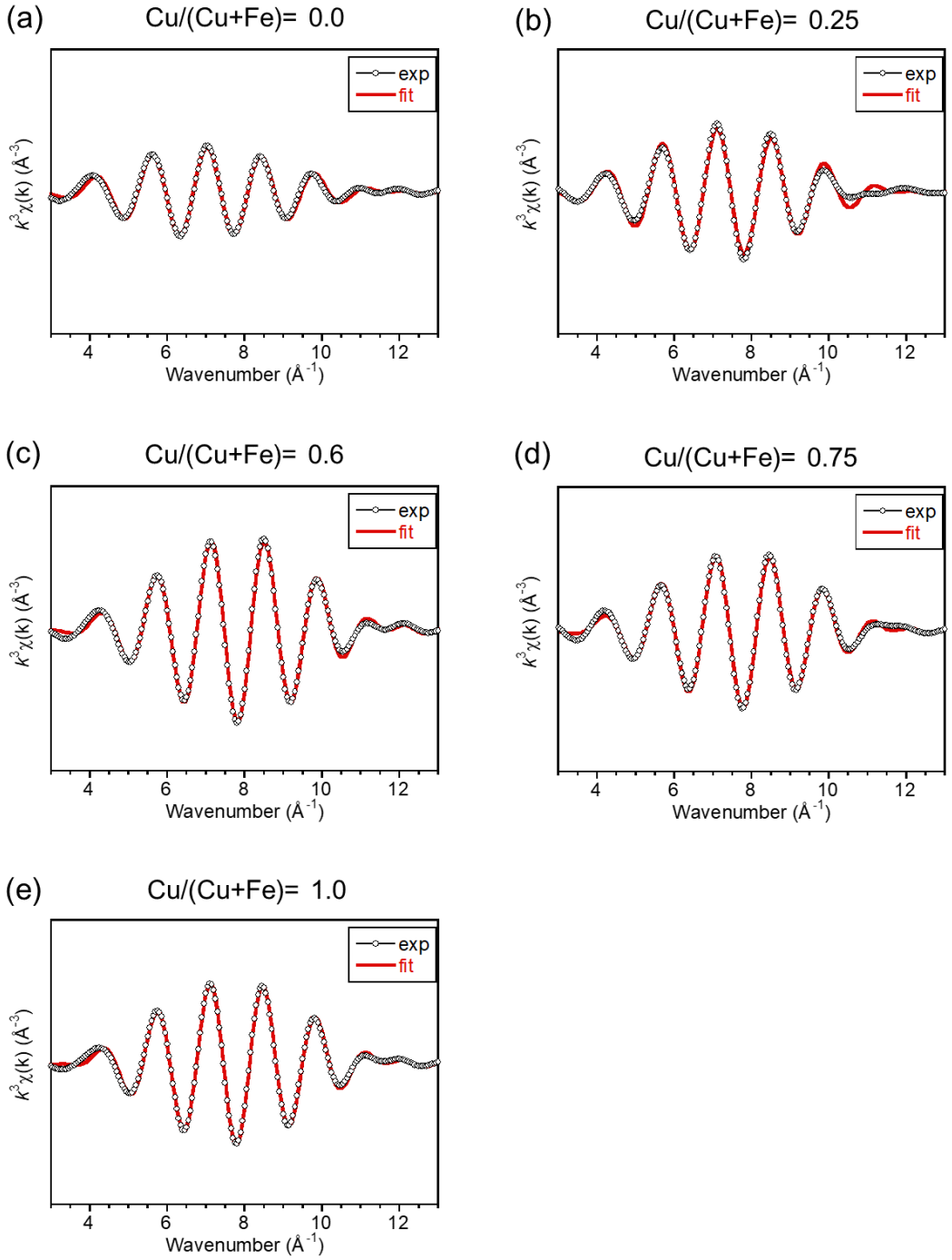

Fig. S20 Fitting details in a q-space for Pt L_{III}-edge EXAFS spectra of a series of Pt–FeCu SAAs with different Cu/(Cu+Fe) molar ratios: Cu(Cu+Fe)= (a) 0.0, (b) 0.25, (c) 0.6, (d) 0.75, (e) 1.0.

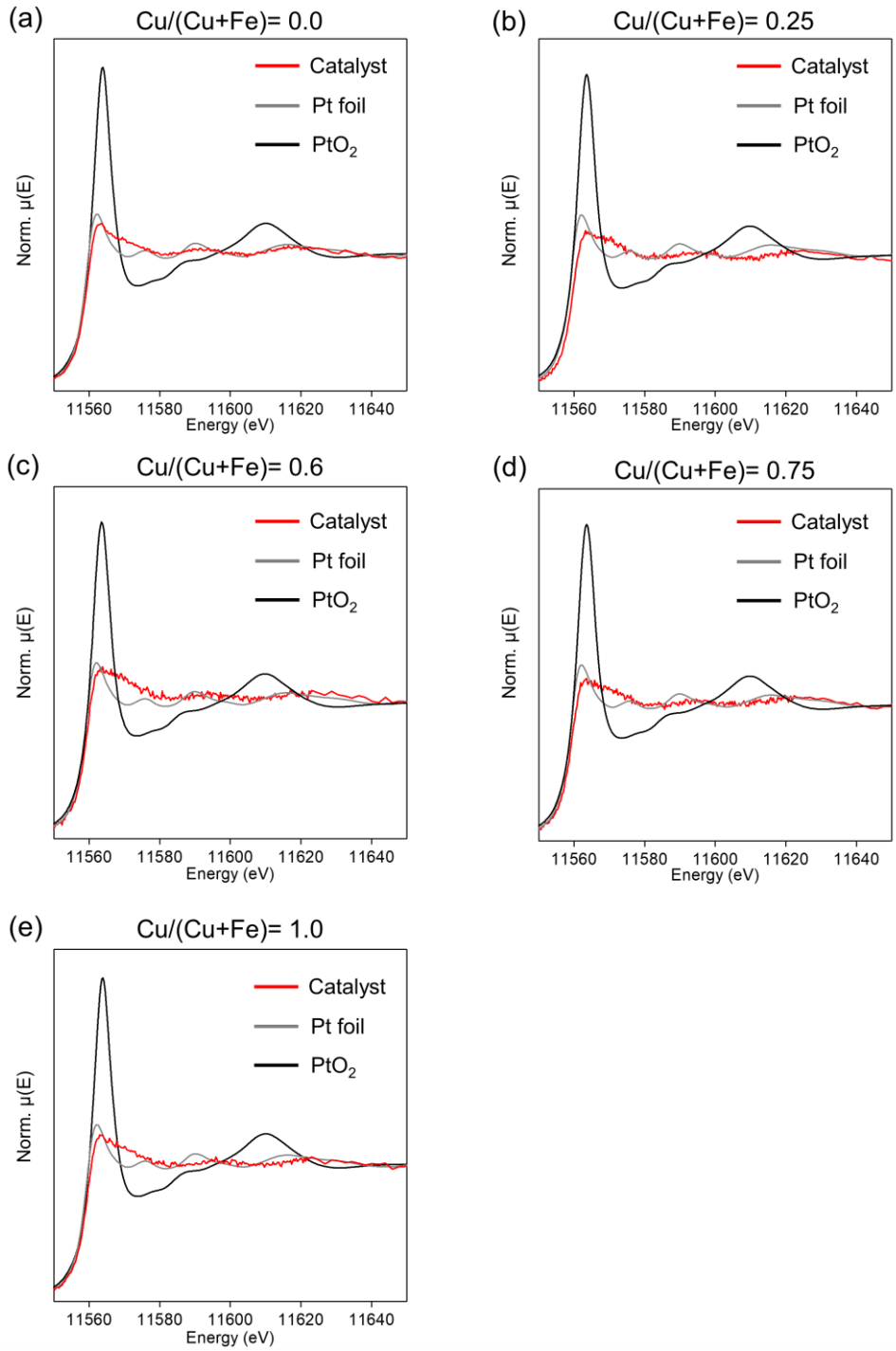

Fig. S21 Pt L_{III}-edge XANES spectra of a series of Pt–FeCu SAAs with different Cu/(Cu+Fe) molar ratios: Cu(Cu+Fe)= (a) 0.0, (b) 0.25, (c) 0.6, (d) 0.75, (e) 1.0.

Table S1. Ladings of each metal used in the catalyst preparation process. ICP results of the prepared catalysts are also given.

Composition at the catalyst preparation Processes				Composition determined by ICP			
Cu/(Cu+Fe) molar ratio	Loading (wt%)			Cu/(Cu+Fe) molar ratio	Loading (wt%)		
	Pt	Fe	Cu		Pt	Fe	Cu
0	0.1	6.0	0.0	0.00	0.056	6.48	0.00
0.25	0.1	9.0	3.0	8.86	0.068	9.09	3.22
0.6	0.1	4.8	7.2	4.36	0.061±0.003[a]	4.40±0.34 [a]	7.70±0.55 [a]
0.75	0.1	3.0	9	2.44	0.064	2.33	9.09
1.0	0.1	0.0	6	0.00	0.063	0.00	5.92

[a] The Pt–FeCu SAA with Cu/(Cu+Fe) molar ratio of 0.6 was prepared three times and their compositions were analyzed. Average values with errors estimated from the three measurements are shown in this table.

Table S2. Atomic ratios of Fe and Cu for Pt–FeCu SAA estimated by XPS and ICP. Fe/Cu contents used in the catalyst preparation, *Theory*, are also given for comparison.

Procedure	Atomic ratio (%)		Cu/(Cu+Fe) molar ratio
	Cu	Fe	
XPS	51.5	48.5	0.52
ICP	63.6	36.4	0.64
Theory	60	40	0.60

Table S3. Structural parameters obtained by curve fitting analysis on the q-space of the EXAFS function.

Parameters	Cu/(Cu+Fe)				
	0.0	0.25	0.6	0.75	1.00
CN	5.3±1.3	5.4±1.1	7.7±0.9	7.4±1.0	7.8±0.9
R (Å)	2.61±0.02	2.58±0.01	2.58±0.01	2.58±0.01	2.60±0.01
σ^2 (Å^2)	0.011±0.002	0.008±0.002	0.008±0.001	0.009±0.001	0.009±0.001

3. Supporting discussion

3.1. Reason why Pt agglomeration is suppressed on Fe surface.

We additionally performed DFT calculations for further understanding of why Pt aggregation can be inhibited on the Fe surface (**Fig. S7**). First, a bcc-Fe(110) slab model with two Pt single-atoms alloyed on the surface was constructed (model a). Next, the local minima of the process of the diffusion of one of the Pt single atoms on the Fe surface and interacting with the remaining Pt single atom were modeled (models b-c). The relative energies of these models were calculated and compared. Based on the obtained data, we discuss whether or not Pt single atoms can be formed on the Fe surface.

The structural model (a) was the most stable. The transition from (a) to (b) required at least 178 kJ/mol of energy (i.e., model (b) is less stable than model (a) by 178 kJ/mol). In model (b), Pt1 is bound to 4 atoms of surface Fe, and Pt2 is bound to 8 atoms of Fe. That is, four Pt–Fe bonds were broken, and vacancy was formed during the geometrical change from model (a). This means that the cleavage of the Pt–Fe bonds at the initial position of Pt1 (model a) is energetically unfavorable. The geometrical change from (b) to (c) additionally required 61 kJ/mol of energy. It is noteworthy that model (c) was less stable than model (b), even though the Pt1–Pt2 bond was formed. This datum indicates the interaction energy of Pt–Pt is smaller than that of Pt–Fe on the Fe surface.

Accordingly, the above computational data suggest that Pt is less likely to aggregate on the Fe surface. This is consistent with the fact that Pt single atoms were observed experimentally.

3.2. On the assignment of thin layer.

Based on the general knowledge in the field of catalysts, it is expected that there are four possible forms; please refer to **Fig. S15**: (a) Fe overlayers on Cu nanoparticles (our model); (b) Cu overlayers on Fe nanoparticles; (c-d) TiO_x-overlayers on Fe/Cu nanoparticles. We can verify their validity based on experimental data. The possibility of (b) can be excluded from the consideration because of the absence of the ν_{CO} band assignable to Cu^0−CO in the CO-FTIR spectrum as discussed in the main text. This is conclusive evidence for the negligible fraction of the surface Cu. Possibility (c-d), which is derived from the strong metal support interaction (SMSI),[17] can be also eliminated from the consideration based on the CO-FTIR data. If the SMSI-derived TiO_x-film is formed on supported nanoparticles and it stabilizes Pt single atoms, $Pt^{\delta+}$ should be formed via electron transfer interaction with the TiO_x overlayer. This kind of $Pt^{\delta+}$ species is distinguishable from the Pt SAAs by CO-FTIR due to the significantly different electronic structures, which has been proven in the literature.[18] In short, TiO_2-supported $Pt^{\delta+}$ single atoms give ν_{CO} band at around 2110−2090 cm^{-1}, whereas Pt SAAs provide ν_{CO} band in a range of 2050−2020 cm^{-1}.[19-20] In the present system, we have performed CO-FTIR spectroscopy toward Pt–FeCu SAA and confirmed that the former-derived band (ν_{CO} band assignable to $Pt^{\delta+}$ single atoms detectable at around 2110–2090 cm^{-1}) is not observable; see **Fig. 5** in the main text. It was just only Pt^0 single atoms that were detected by the CO-FTIR spectroscopy. Furthermore, Pt L_{III}-edge WT-EXAFS provided no Pt–O backscattering (**Fig. 4d**). Pt L_{III}-edge XANES spectrum showed zero valence state equivalent with Pt foil (**Fig. 4c**). Therefore, the possibility of the thin layer of TiO_2-supported Pt single-atoms over nanoparticles, i.e., models (c-d) in **Fig. S15**, can be excluded from the consideration.

Through the above discussion, only a possibility of (a) remains. Based on the experimental results including CO-FTIR, XAFS, and XPS (despite ex situ) with the literature findings (Fe would be spontaneously migrated on the supported Cu nanoparticles), which are discussed in the manuscript, we can reasonably claim that the thin layer detected by HAADF-STEM images can be assigned to the Fe overlayers.

4. Supporting references

1. A. Oda, T. Fujita, Y. Yamamoto, K. Sawabe, A. Satsuma, *ACS Catal.* 2023, 13, 10026-10040.
2. K. Murata, N. Kurimoto, Y. Yamamoto, A. Oda, J. Ohyama, A. Satsuma, *ACS Applied Nano Mater.* 2021, **4,** 4532-4541.
3. B. Ravel, M. Newville, *Physica Scripta* 2005, **2005,** 1007.
4. H. Funke, A. Scheinost, M. Chukalina, *Phys. Rev. B* 2005, **71,** 094110.
5. H. Funke, M. Chukalina, A. C. Scheinost, *J. Synchrotron Radiat.* 2007, **14,** 426-432.
6. G. Kresse, J. Hafner, *Phys. Rev. B* 1993, **48,** 13115.
7. G. Kresse, J. Hafner, *Phys. Rev. B* 1994, **49,** 14251.
8. G. Kresse, J. Furthmüller, *Phys. Rev. B* 1996, **54,** 11169.
9. G. Kresse, J. Furthmüller, *Comput. Mater. Sci.* 1996, **6,** 15-50.
10. P. E. Blöchl, *Phys. Rev. B* 1994, **50,** 17953.
11. G. Kresse, D. Joubert, *Phys. Rev. B* 1999, **59,** 1758.
12. J. P. Perdew, Y. Wang, *Phys. Rev. B* 1992, **45,** 13244.
13. J. P. Perdew, K. Burke, M. Ernzerhof, *Phys. Rev. Lett.* 1996, **77,** 3865.
14. S. Grimme, J. Antony, S. Ehrlich, H. Krieg, *J. Chem. Phys.* 2010, **132,** 154104.
15. S. Grimme, S. Ehrlich, L. Goerigk, *J. Comput. Chem.* 2011, **32,** 1456-1465.
16. K. Momma, F. Izumi, *J. Appl. Crystallogr.* 2011, **44,** 1272-1276.
17. S. Zhang, P. N. Plessow, J. J. Willis, S. Dai, M. Xu, G. W. Graham, M. Cargnello, F. Abild-Pedersen, and X. Pan, *Nano Lett*. 2016, **16,** 4528−4534.
18. L. DeRita, S. Dai, K. Lopez-Zepeda, N. Pham, G. W. Graham, X. Pan, P. Christopher, *J. Am. Chem. Soc.* **2017,** *139*, 14150-14165.
19. D. L. Molina, M. Inagaki, E. Kazuma, Y. Kim and M. Trenary, *J. Phys. Chem. C*, 2023, **127**, 9796-9806.
20. A. Mohammadpour and S. Kaya, *J. Phys. Chem. C*, 2024, **128,** 5480–5489.